Supporting Information

Cideciyan *et al.* 10.1073/pnas.0807027105

SI Text

Photoreceptor Layer Topography. Optical coherence tomography scans were obtained with an ultra-high speed (26,000 A-scans per second) and high-resolution (5 μm axial, 15 μm lateral) Fourier-domain system (RTVue-100; Optovue). Two scanning patterns were used: line scans (4096 A-scans covering 4.5 mm) and raster scans (101 raster lines of 512 A-scans each covering 6 × 6 mm). Multiple overlapping line scans were used to obtain higher-resolution coverage along horizontal and vertical meridians up to 9 mm eccentricity from the fovea (1–4). Similarly multiple overlapping raster scans were used to sample an 18 × 12 mm rectangular region of the retina centered on the fovea (3, 5, 6). Postacquisition processing of data was performed with custom programs (MatLab 6.5; MathWorks). Lateral sampling density of the line scans were reduced by averaging groups of eight neighboring A-scans to increase signal-to-noise ratio, aligned using a dynamic cross-correlation algorithm (7), and digitally stitched along the horizontal and vertical meridians. Two nuclear layers, the ONL and the inner nuclear layer, were defined in regions of scans showing two parallel stereotypical hyporeflective layers sandwiched between the RPE and vitreoretinal interface, and extended laterally to regions with thinner ONL. The boundary of the outer hyporeflective layer corresponding to the ONL was defined by the minima/maxima of the signal slope. For topographic analysis, original raster sets were sub-sampled down to 21 lines after discarding artefactual lines corresponding to blinks and eye movements. The precise location and orientation of each raster line was determined relative to retinal features using video images of the fundus. A-scans were allotted to regularly spaced bins (0.3 × 0.3 mm) in a rectangular coordinate system centered at the fovea; the waveforms in each bin were aligned and averaged. ONL thickness was measured from averaged A-scans in each bin as described earlier. Missing data were interpolated bi-linearly, thickness values were mapped to a pseudocolor scale, and locations of blood vessels and optic nerve head were overlaid for reference.

Psychophysical Studies. Absolute visual sensitivity to stimuli under dark-adapted conditions was determined with a modified computerized perimeter (Humphrey Field Analyzer; Zeiss Meditec) as published (1, 8–11). The achromatic (white) stimulus was 1.7° in diameter and 200 ms in duration (maximum luminance, 3,180 cd·m^{-2}), presented along the vertical or horizontal meridians crossing fixation. Tests were performed at several pretreatment time points ranging from 3 to 24 months before surgery and at three posttreatment time points of day 30, 60, and 90. Retinal loci were typically sampled at 0.6 mm intervals up to 9 (vertical) or 18 (horizontal) mm eccentricity from the fixation. All extrafoveal loci were tested using a red fixation target with a variable intensity adjusted to be visible for each subject. Foveal sensitivities were determined while gazing at the center of four red lights forming a diamond. Sensitivity values were spatially smoothed using a three-point moving average; foveal sensitivities were reported without spatial averaging. Locus-by-locus differences were calculated between posttreatment and pretreatment results. The statistical significance of the difference calculated at each locus was defined by comparison to the maximum expected test–retest variability. To obtain the most conservative estimates, the best pretreatment sensitivity was used for defining loci with significant improvement and the worst pretreatment sensitivity was used for defining loci with significant deterioration. The maximum expected test–retest variability limit (3 SD = 0.80 log units) was based on the range of sensitivities obtained in patients with *RPE65*-LCA (n = 8) who were each tested two or three times on consecutive days. For the variability estimates, if data were available from both eyes of a subject, the eye with the worse visual acuity was used. All locations with a zero sensitivity and their immediate neighbors were not included in this analysis to avoid artefactual reduction of variability that may occur in regions with severe vision loss as a result of the "floor effect," whereby data are forced to the lowest number (i.e., highest light intensity) available by the instrument. Coincidentally, the test–retest limit calculated in patients with *RPE65*-LCA was similar to the limit (i.e., 3 SD) of interindividual variability (0.72 log units) observed in normal subjects.

In retinal regions with evident biological activity, dark adaptation testing was performed to define the rod and cone visual cycle kinetics (12–19). A yellow full field–adapting light exposure of 7 log scot-td·s was delivered with a flash unit mounted at the top of a 150-mm-diameter sphere with a white inner coating and an opening for the subject's eye. In a fully dark-adapted healthy eye, ≈60% of the available rhodopsin molecules would be expected to absorb a primary quantum with this flash. The adapting flash was delivered under near-infrared (NIR) viewing of the subject's pupil to avoid reduction in retinal exposure caused by partially closed eyelids. During testing, NIR LEDs illuminated the pupil and an NIR-sensitive camera allowed continuous monitoring of pupil position. The stimuli used were blue or red LEDs illuminating an opal diffuser (1.7° diameter); for testing healthy eyes, a three–log unit neutral density filter was intercalated between the blue LED and the diffuser to shift the whole dynamic range of the instrument to lower illuminances. Under software control, LEDs were driven with amplitude and pulse-width modulation to achieve a 5.8 log unit dynamic range. Thresholds to blue and red stimuli were determined using a staircase procedure before and at regular intervals after the adapting flash. Differences between the sensitivities to blue and red stimuli were used to determine the type of photoreceptor mediating vision. Log-linear segments of rod-mediated recovery were fit with lines to estimate exponential time constants.

In addition, two-color perimetry (blue, 500 nm; red, 650 nm) was performed during the cone-plateau period following the adapting flash and/or under standard (1–2 h) and extended (3–8 h) dark adaptation conditions to understand the retinal distribution of cone- and rod-mediated vision across the treated areas. Patient 1 could not perceive the highest intensity available with the standard-sized chromatic stimuli. Therefore, larger (4° diameter) blue (500 nm), orange (600 nm), and red (650 nm) stimuli were used posttreatment to estimate type of photoreceptor mediation within his region of biological activity. Pretreatment, one of the patients (patient 2) could perceive chromatic stimuli only to eccentricities <3 mm; the other two patients could not perceive the stimuli at any extrafoveal locus. Thus, pretreatment cone- and rod-mediated vision was estimated from achromatic sensitivities using the most conservative assumption that both rods and cones were contributing to this very low level of vision.

Fixation Location and Stability Studies. Preferred retinal locus used by patients with *RPE65*-LCA to fixate to a stationary target and the stability of fixation were determined by video imaging of the retina under NIR light and recording the movement of each video image obtained at a 25-Hz rate with respect to a reference image (MP1; Nidek Technologies America). Recordings were

monocular (eyes were tested sequentially) and performed during a fixation task involving visualization of a red target; the total length of recording was 45 seconds. The fixation light was ≈3 log units brighter than normal perceptual threshold, and all patients tested could see the target throughout the recording period. The movement of the retinal image with respect to the fovea was recorded as horizontal and vertical offset values as a function of time. A representative 10-s epoch was selected; horizontal and vertical offsets were converted to radial distances and the SD of these radial distances over the 10-s epoch was reported as a measure of fixation instability (2).

Pupillometry Studies. The direct transient pupillary light reflex (TPLR) was elicited and recorded (20, 21). TPLR luminance-response functions were derived from responses to increasing intensities (from −6.6 to 2.3 log scot-cd·m^{-2}) of green stimuli with short duration (0.1 s) presented monocularly in the dark-adapted state. The light stimulated pupil was imaged with an infrared-sensitive video camera (LCL-903HS; Watec America) and images were digitized by two instruments simultaneously. A digital image processor (RK-706PCI, ver. 3.55; Iscan) sampled the horizontal pupil diameter at 60 Hz and a video digitizer (PIXCI SV4 board, ver. 2.1; Epix) produced a computer file of the video sequence. Records were 5.7 s long, with a 1-s pre-stimulus baseline. TPLR amplitude was defined as the difference between the pupil diameter at a fixed time (0.9 s) after the onset of the stimulus and the pre-stimulus baseline. TPLR response threshold was defined as the stimulus luminance that evoked a criterion (0.3 mm, limit of spontaneous oscillations in pupil diameter, ref. 20) contraction of the pupil diameter at the fixed time (0.9 s) considered.

Animal Studies. Naturally occurring *Rpe65*-mutant *rd12* mice (n = 20) were used. Procedures were conducted in accordance with the ARVO Statement for the Use of Animals in Ophthalmic and Visual Research and with institutional approval. Breeding, origins, maintenance before and after surgery, and surgical details have been described (22, 23). In the first set of experiments, a single 1-μl subretinal injection of the rAAV2-CB^{SB}-h*RPE65* vector, which remained in the syringe after each human surgery, was delivered subretinally to one eye of *rd12* mice (ages 17–52 d). The non-injected eyes of the same animals served as controls. ERG recordings were performed 25 to 37 days after the injection. In a second set of experiments, *rd12* mice were used to study early effects of uniocular subretinal injection of rAAV2-CB^{SB}-h*RPE65* vector (n = 2) and of BSS vehicle (n = 2). Non-injected eyes of the same animals served as controls. ERG recordings were performed at 10 days after the injections. In both experiments, full field bilateral ERGs were recorded as described (23). Animals were dark-adapted (>12 h) and anesthetized with intramuscular ketamine HCl (65 mg/kg) and xylazine (5 mg/kg); corneas were anesthetized with proparacaine HCl, and pupils dilated with tropicamide (1%) and phenylephrine (2.5%). Responses evoked by a 0.1 log scot-cd·s·m^{-2} flash were amplified, filtered (−3 dB cutoff at 0.3 and 300 Hz) and digitized (2 kHz) with a 12-bit analog-to-digital converter. B-wave amplitudes were measured conventionally, from baseline or a-wave trough to positive peak, and vector-injected eyes were plotted against non-injected fellow eyes. Existence of a significant efficacy resulting from vector was defined in each animal by comparison to the expected variability (i.e., 3 SD) of interocular differences of this waveform amplitude in untreated *rd12* and WT eyes (23). To test for the possibility that preformed RPE65 protein—either contained within the vector capsid or adhering to its surface—was responsible for the rapid therapeutic response seen in these mice, we performed an hRPE65 ELISA on 10 μl of undiluted test vector (1.4×10^{13} vector genomes per ml) diluted in 90 μl of coating buffer containing 2% SDS, then boiled for 5 min before coating the ELISA plate. For the positive control, ELISA wells were coated with 0.5 μg/well hRPE65 protein expressed from *Escherichia coli* and pretreated as for the test vector. Anti-RPE65 monoclonal antibody (1 mg/ml) (Chemicon, cat# MAB 5428) at a dilution of 1:640,000 was used to detect hRPE65 in all wells and to generate the highest point in a standard curve. No hRPE65 was detected in clinical vector samples or in similar preclinical vector within the limits of the assay (data not shown), suggesting that expression from the hRPE65 transgene after delivery to the RPE by vector most likely accounts for the rapid therapeutic response.

1. Jacobson SG, *et al.* (2005) Identifying photoreceptors in blind eyes caused by RPE65 mutations: prerequisite for human gene therapy success. *Proc Natl Acad Sci USA* 102:6177–6182.
2. Jacobson SG, *et al.* (2007) Human cone photoreceptor dependence on RPE65 isomerase. *Proc Natl Acad Sci USA* 104:15123–15128.
3. Aleman TS, *et al.* (2007) Inner retinal abnormalities in X-linked retinitis pigmentosa with RPGR mutations. *Invest Ophthalmol Vis Sci* 48:4759–4765.
4. Aleman TS, *et al.* (2008) Retinal laminar architecture in human retinitis pigmentosa caused by rhodopsin gene mutations. *Invest Ophthalmol Vis Sci* 49:1580–1590.
5. Cideciyan AV, *et al.* (2007) Centrosomal-ciliary gene CEP290/NPHP6 mutations result in blindness with unexpected sparing of photoreceptors and visual brain: implications for therapy of Leber congenital amaurosis. *Hum Mutat* 28:1074–1083.
6. Jacobson SG, *et al.* (2008) Photoreceptor layer topography in children with Leber congenital amaurosis caused by *RPE65* mutations. *Invest Ophthalmol Vis Sci*, in print
7. Huang Y, *et al.* (1998) Relation of optical coherence tomography to microanatomy in normal and rd chickens. *Invest Ophthalmol Vis Sci* 39:2405–2416.
8. Jacobson SG, *et al.* (1986) Automated light- and dark-adapted perimetry for evaluating retinitis pigmentosa. *Ophthalmology* 93:1604–1611.
9. Jacobson SG, Yagasaki K, Feuer W, Roman AJ (1989) Interocular asymmetry of visual function in heterozygotes of X-linked retinitis pigmentosa. *Exp Eye Res* 48:670–691.
10. Van Hooser JP, *et al.* (2000) Rapid restoration of visual pigment and function with oral retinoid in a mouse model of childhood blindness. *Proc Natl Acad Sci USA* 97:8623–8628.
11. Jacobson SG, *et al. (2007) RDH12* and. *RPE65*, visual cycle genes causing Leber congenital amaurosis, differ in disease expression *Invest Ophthalmol Vis Sci* 48:332–338.
12. Jacobson SG, *et al.* (1995) Night blindness in Sorsby's fundus dystrophy reversed by vitamin A. *Nat Genet* 11:27–32.
13. Cideciyan AV, Pugh EN Jr, Lamb TD, Huang Y, Jacobson SG (1997) Rod plateaux during dark adaptation in Sorsby's fundus dystrophy and vitamin A deficiency. *Invest Ophthalmol Vis Sci* 38:1786–1794.
14. Cideciyan AV, *et al.* (1998) Null mutation in the rhodopsin kinase gene slows recovery kinetics of rod and cone phototransduction in man. *Proc Natl Acad Sci USA* 95:328–333.
15. Cideciyan AV, *et al.* (1998) Disease sequence from mutant rhodopsin allele to rod and cone photoreceptor degeneration in man. *Proc Natl Acad Sci USA* 95:7103–7108.
16. Cideciyan AV, *et al.* (2000) Rod and cone visual cycle consequences of a null mutation in the 11-cis-retinol dehydrogenase gene in man. *Vis Neurosci* 17:667–678.
17. Poehner WJ, *et al.* (2000) A homozygous deletion in RPE65 in a small Sardinian family with autosomal recessive retinal dystrophy. *Mol Vis* 6:192–198.
18. Jacobson SG, Cideciyan AV, Wright E, Wright AF (2001) Phenotypic marker for early disease detection in dominant late-onset retinal degeneration. *Invest Ophthalmol Vis Sci* 42:1882–1890.
19. Cideciyan AV, *et al.* (2004) Mutations in ABCA4 result in accumulation of lipofuscin before slowing of the retinoid cycle: a reappraisal of the human disease sequence. *Hum Mol Genet* 13:525–534.
20. Aleman TS, *et al.* (2004) Impairment of the transient pupillary light reflex in Rpe65-/- mice and humans with Leber congenital amaurosis. *Invest Ophthalmol Vis Sci* 45:1259–1271.
21. Aguirre GK, *et al.* (2007) Canine and human visual cortex intact and responsive despite early retinal blindness from RPE65 mutation. *PLoS Med* 4:e230.
22. Pang JJ, *et al.* (2005) Retinal degeneration 12 (rd12): a new, spontaneously arising mouse model for human Leber congenital amaurosis (LCA). *Mol Vis* 11:152–162.
23. Roman AJ, *et al.* (2007) Electroretinographic analyses of Rpe65-mutant rd12 mice: developing an in vivo bioassay for human gene therapy trials of Leber congenital amaurosis. *Mol Vis* 13:1701–1710.

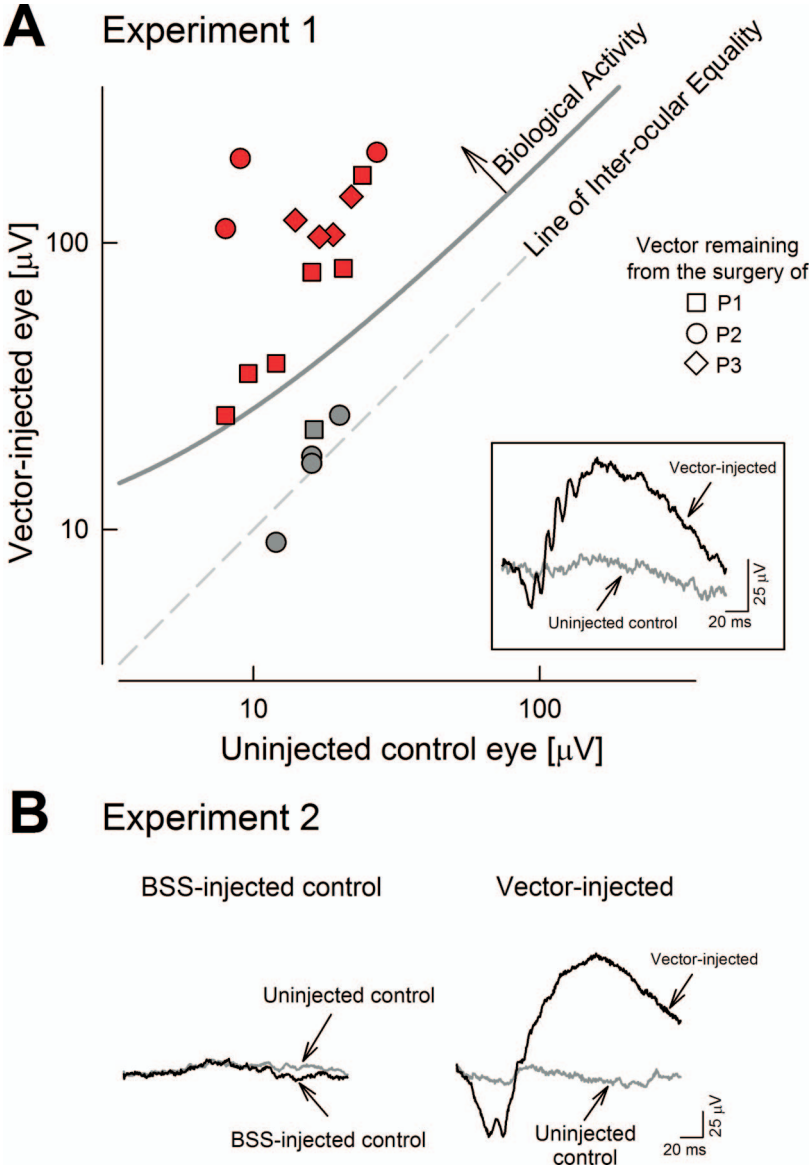

Fig. S1. Hypothesis testing regarding human results after treatment using the *rd12* mouse model of Rpe65 deficiency. (*A*) In experiment 1, *in vivo* bioassay of the gene therapy vector used in human surgery shows biological activity. Electroretinographic (ERG) b-wave amplitudes in vector-injected eyes versus non-injected control eyes of *rd12* mice. Vector (1 μl) is from the syringe used in the surgery of each *RPE65*-LCA subject (patient 1, squares; patient 2, circles; patient 3, diamonds). Dashed line of equality corresponds to no interocular difference in this ERG parameter. Solid line defines upper limit of significant interocular difference (3 SD) derived from untreated *rd12* and WT animals. Thirteen treated eyes (red symbols) showed a significant ERG improvement in the treated eyes, whereas five (gray symbols) did not. Significant ERG improvements provide evidence of the biologic activity of the vector used for each patient; small subset of failures are attributed to the surgical uncertainty of delivering vector unerringly to the subretinal space in the small mouse eye. (*Inset*) ERG waveform from a vector-injected (black trace) versus the non-injected control eye (gray trace) of an *rd12* mouse from this experiment. (*B*) In experiment 2, robust biological activity is observable as early as 10 days after injection. Representative ERG waveforms 10 days after subretinal injection of vector (*Right*; black traces) or vehicle (*Left*; black traces) compared with non-injected control eyes (gray traces). These results suggest that surgical detachment of the retina with a subretinal injection not containing vector does not cause an ERG improvement.

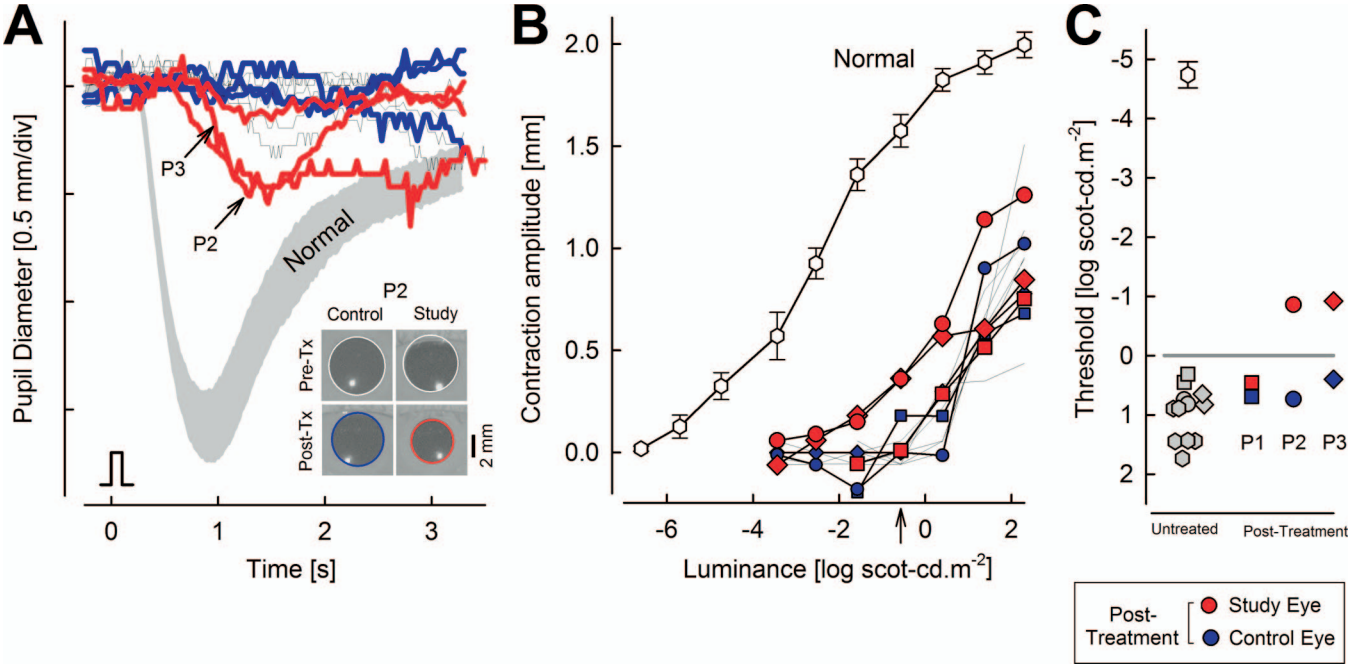

Fig. S2. Pupillary responsivity increases after treatment. (*A*) Change in pupil diameter evoked by a short duration light stimulus (0.1 s, −0.6 log scot-cd·m^{-2}, green, dark-adapted) in study and control eyes of the three patients at 18 months before treatment (thin black traces) and 1 month after treatment (red, study eye; blue, control eye) compared with results from normal subjects (gray band, mean ± 2 SEM; $n = 13$). Pretreatment eyes do not show changes in pupil diameter that are distinguishable in magnitude (<0.3 mm) from spontaneous oscillations of the pupil diameter of the dark-adapted eye. Posttreatment (red) traces show sizable pupil contractions in the study eyes of two of the patients (patients 2 and 3) but not in patient 1. Pupils from control eyes (blue traces) after treatment do not contract in response to this stimulus. Stimulus monitor trace at the bottom left. (*Inset*) Video frames of pupils of control and study eyes of patient 2 at 0.9 s after the light stimulus; pupillary margin is outlined in white (pretreatment), red (posttreatment, study eye), or blue (posttreatment, control eye) for visibility; calibration bar at the bottom right. (*B*) Luminance response functions measured at 0.9 s after stimulus onset in both eyes of each patient before treatment (thin black lines) and after treatment in the study eye (red) compared with the control eye (blue) and with normal data (mean ± SEM, white symbols). Before treatment (thin black lines), pupil contractions were observed only with the two highest luminance stimuli. After treatment (red symbols), there were contractions in the study eye of patients 2 and 3 within a range of stimuli and there was a shift of the luminance response function to the left; no such responding was recorded in patient 1 or in the control eyes. Arrow points to stimulus luminance of the waveforms shown in *A*. (*C*) Pupillary response thresholds in patients with untreated *RPE65*-LCA (gray hexagons, other *RPE65*-LCA patients; gray squares, patient 1; gray circles, patient 2; gray diamonds, patient 3) show abnormalities in excess of 5 log units compared with normal (white hexagon, mean ± 2 SD). Thresholds in the study subjects before treatment are similar to each other and to other patients with *RPE65*-LCA (gray hexagons, $n = 3$; gray line, mean ± 2 SD for untreated *RPE65*-LCA). The treated eye of patient 2 improved by 1.6 log units, from 0.74 log scot-cd·m^{-2} before treatment to −0.86 log scot-cd·m^{-2} after treatment (red). Patient 3 improved by 1.8 log units from 0.83 log scot-cd·m^{-2} before treatment to −0.92 log scot-cd·m^{-2} after treatment. The untreated eyes did not change (blue symbols). Patient 1 showed no detectable changes, which may be attributed to the smaller increase in posttreatment visual sensitivity compared with patients 2 and 3.

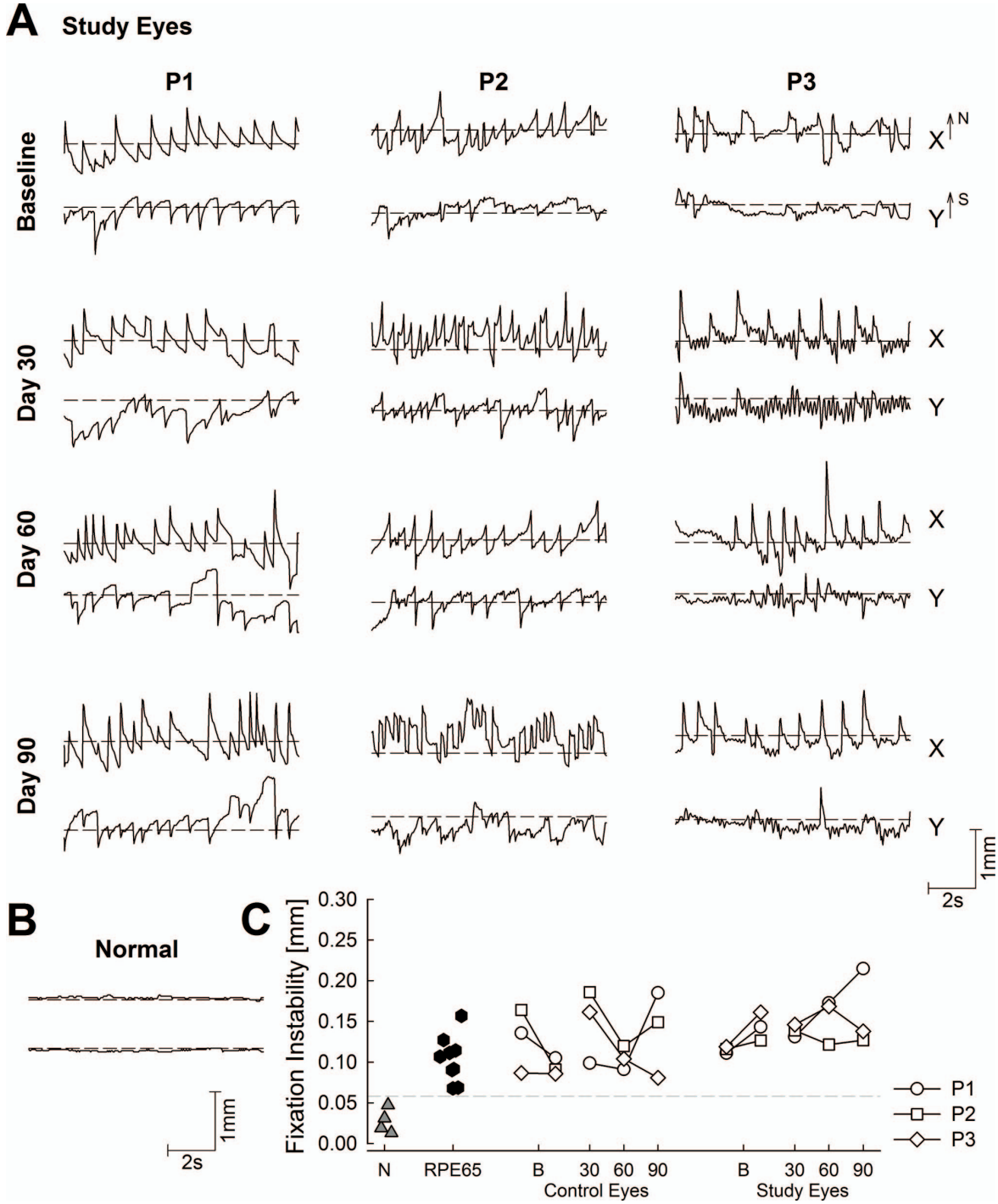

Fig. S3. Fixation location and fixation stability of control and study eyes do not change after treatment. (*A*) Pairs of traces show the x- and y-axis deflections of the location of the fovea recorded with infrared fundus imaging over 10-s epochs in the study eyes of three patients at baseline and days 30, 60, and 90 after treatment. Control eyes showed similar results (not shown). Horizontal dashed lines are the reference location of the fovea at the start of the recording session 15–35 s preceding the selected epoch. All patients show abnormal eye movements with horizontal and vertical components of instability and larger amplitude jerk nystagmus occurring at frequencies of ≈1–2 Hz. All plots are shown as equivalent left eyes for clarity and consistency with other figures. (*B*) Traces from a representative normal subject. (*C*) Summary of fixation instability in all subjects. Horizontal dashed line is a conservative (+3 SD) upper limit of normal (N) from the mean value. Study and control eyes of patients 1, 2, and 3 at two baseline (B) visits show fixation instability similar to other patients with *RPE65*-LCA (dark hexagons). At posttreatment days 30, 60, and 90, there are no consistent increases or decreases in fixation instability for the study and control eyes.